Chapter 4

The Nucleus of Comet Hale-Bopp

4.1 Background

Comet Hale-Bopp, discovered in July of 1995, likely was the most watched comet in all of history. A prodigious producer of dust and gas and a marginally advantageous orbital geometry combined to provide quite a show for several months in early 1997. However, all of that gas and dust made it exceedingly difficult to measure the nucleus; the continuum of the comet was dominated by the dust grains in the optical and mid-IR regimes. Two unusual techniques helped to partially sidestep this problem – the observation of an occultation of a star by the comet, and the measurement of the microwave continuum. The latter has been discussed briefly in Chapter 2. The former I will describe in detail here, with text heavily borrowed from a paper I wrote (Fernández *et al.* 1999).

4.2 Occultation Measurements

4.2.1 Introduction

Since the length scales of the nuclei and inner comae of comets are so small, stellar occultations hold great promise for probing these deep regions at the heart of the comet (see, e.g., Combes *et al.* [1983]). For a comet that is 1 AU away, the ∼10-km length scale subtends less than $0.02''$, or less than half the width of a pixel on the Planetary Camera of *HST*'s WFPC2. Unfortunately, there are only a few published reports of observed occultations by comets, and the reported chords have not come particularly close to the nuclei. The extinction of the star has been found to be a few percent at a distance of several hundred kilometers from the nucleus for comets of various activity levels and dust-to-gas ratios (e.g., Larson and A'Hearn 1984, and Lecacheux *et al.* 1984). One comet has been the target of an occultation observation with an impact parameter so small that the star was occulted by the nucleus itself, not just the coma: 95P/(2060) Chiron (Bus *et al.* 1996). Of course the very low activity, large nucleus, and regular orbit of this object mark this as a special case.

Though most previous data on cometary occultations were obtained at permanent observatories, with a sufficient number of portable telescope systems spaced across a territory over which an occultation is predicted to occur, as we have done

here, one can in principle obtain a size and shape estimate of the nucleus – independent of the albedo ambiguity found in optical photometry – and an estimate of the opacity structure of the coma to learn about the dynamics and scattering properties of the dust.

It is worthwhile to emphasize the differences between observing comet occultations and the much more common asteroid counterparts. While an asteroid is a point source, located near the center of brightness, and usually on a well-defined path (making the prediction uncertainty just a few shadow widths), a cometary nucleus is often swamped by coma emission of an uncertain morphology, making it hard to decide exactly where the nucleus is within the comet image's brightest pixel. (This is especially true for Hale-Bopp, the dustiest comet on record.) Moreover, nongravitational forces push the comet away from the ephemeris position (although fortunately this is probably not a problem for Hale-Bopp). There are even potentially significant errors in the ephemeris itself, since it is usually derived from astrometry of the comet's brightest spot, not the nucleus' location. Lastly the typical comet nucleus is only a few kilometers wide. The result is to make observing cometary occultations more logistically difficult than observing their asteroid counterparts.

Here I report the observation of the dimming of star PPM 200723 due to its occultation by Comet Hale-Bopp (C/1995 O1). (The star is also known as SAO 141696, BD -04 4289, and GSC 5075-0004.) Barring a terrestrial explanation, the star's light was completely or nearly completely blocked along part of one occultation chord, implying that a line of sight through an optically thick portion of the inner coma, or through the nucleus itself, was observed. On two other chords, no significant diminution of light was observed. If our interpretation is correct, this is the closest to the nucleus a typical comet has ever been sampled via a stellar occultation. I will give results from analyses of the data from this unique observation in the following sections.

4.2.2 Observations

The circumstances of the 5 October 1996 (UT) event are given in Table 4.1. The occultation path (uncertain to $\pm$60 s in time and $\pm$700 km in distance) passed through the western United States soon after sunset on 4 Oct. Six portable teams were arrayed across the region and one permanent facility was used; a map is shown in Fig. 4.1 with the location of the teams as crossed-squares. Table 4.2 lists the location, equipment, and data obtained by the seven teams. Each mobile team (1 through 6) had two members; I was part of Team 5. Originally the teams were to spread out from central Nevada northward to maximize the chance that at least one team would record a significant optical depth ($\geq$ 10%) through the coma; clouds covering Washington, Oregon, Idaho, and western Montana during the event dictated where each portable team positioned itself. Sufficient signal during the event was obtained only by Teams 5, 6, and 7: Team 5 recorded a feature that appears to be the event itself through passing cirrus clouds, while observing at the town dump of Snowville, Utah. Team 6 has at best a marginal light curve feature at the appropriate time, and Team 7 did not detect the event.

Table 4.1. Characteristics of Comet Hale-Bopp Occultation

• The Star, PPM 200723	
Magnitude[a,b]	m_V=9.1
MK Spectral Type[b]/Luminosity Class[c]	K0V
J2000 Right Ascension[b]	$17^{\rm h}29^{\rm m}59\overset{\rm s}{.}845$
J2000 Declination[b]	$-4°48'09''.45.$
• The Comet, C/1995 O1 (Hale-Bopp)	
Magnitude (in 24-arcsec wide circular aperture)	m_R =8.5
Heliocentric Distance	2.83 AU
Geocentric Distance	3.00 AU
Distance Scale at Comet	2.18 km $\doteq 10^{-3}$ arcsec
Solar Elongation	71.0°
Phase	19.5°
Proper Motion and PA	8.41 arcsec/hr, 30.6°
Equivalent Linear Speed	5.11 km/s
• The Observing Locale[d]	
Time of mid-event	5 Oct 1996, 03:17:48 UT ±3 s
Speed of Nuclear Shadow	11.6 km/s
Elevation and Azimuth of Comet	25.8°, 235.8°

a Smithsonian Astrophysical Observatory 1966.
b Röser and Bastian 1991.
c Measured by Jeffrey Hall of Lowell Obs. (private communication).
d Specifically, location of Team 5 (see Table 4.2) at the time of event.

Table 4.2. Observations of Occultation by Comet Hale-Bopp

Team	Location	System†		Summary of Results
		CCD	PMT	
1.	44°39′ N 112°05′ W	√		Heavy clouds during event
2.	43°19′ N 114°41′ W	√		Heavy clouds during event
3.	43°05′ N 116°19′ W	√		Heavy clouds during event
4.	42°30′ N 114°47′ W	√		Heavy clouds during event
5.	41°57′ N 112°44′ W		√	Thin clouds, but detection of event
6.	37°12′ N 117°00′ W		√	Clear; marginal detection?
7.	35°06′ N 111°32′ W		√	Clear, but not detection

† Teams 1 through 6 used Celestron C14 14-in (0.35-m) telescopes; Team 7 used the Lowell Observatory 31-in (0.8-m) NURO telescope. Teams with "CCD" used a charge-coupled device. Teams with "PMT" used a photomultiplier tube with effective wavelength near 4000 Å.

The three solid lines in Fig. 4.1 trace out two 100-km wide swaths which show the last pre-event prediction of the occultation track. The true track was only as wide as Hale-Bopp's nucleus (with projection effects), and the swaths do *not* represent the systematic error in the determination of the track's location, which were closer to ± 700 km (1σ). These swaths were used to aid in choosing locations for the portable teams.

The pre-event ephemeris (Solution 41 by D. K. Yeomans of Jet Propulsion Laboratory) predicted an occultation path shown by the long-dashed lines in Fig. 4.1. Astrometric corrections to this path, using images of the comet taken with the U. S. Naval Observatory Flagstaff Station (USNOFS) 1.5-m telescope, moved the predicted track to the short-dashed lines in Fig. 4.1. The coma-fitting technique that I describe in Chapter 3 was employed to find the source of the coma (i.e., the nucleus) within an image of the comet's center of brightness, moving the track to the solid lines in Fig. 4.1. The corrections gave a net shift to the prediction of Yeomans' ephemeris of about 9×10^2 km northwest. Our apparent detection of the nucleus occurred closer to the original prediction than the corrected one, indicating we had underestimated the prediction errors and that our corrections did not reduce the error, only delimit it. As we will show, with all the uncertainties of event prediction (as mentioned in Section 4.2.1), the detection of the occultation ~ 800 km away from the "best" guess is perfectly reasonable.

Weather and equipment problems prevented Team 5 from observing the comet and the star separately to determine their relative brightnesses in the photometer passband. Using the known spectral characteristics of both objects, combined with broad- and narrow-band imaging taken near the day of the event, we estimate the star to be 0.35 ± 0.02 times as bright as the sum of the comet, sky flux, and detector noise. The method is described here.

The bandpass of Team 5's system is shown in Fig. 4.2; all that is needed is the ratio C of star flux to the sum of fluxes from comet, sky, and detector noise within this band and within the 1-arcmin wide aperture that was used. Starting with CCD observations of the comet and star taken with the USNOFS 1.5-m telescope on 2, 3, and 5 Oct 1996. We know the relative brightnesses (to $\pm 5\%$) in their passband, the spectral shape of which is also shown in Fig. 4.2 (Monet *et al.* 1992). To switch to Team 5's band now requires knowing the spectra of the comet and the star.

Fig. 4.2 shows the spectrum of a typical K0V star (Kharitonov *et al.* 1988, Silva and Cornell 1992, Jacoby *et al.* 1984) and of the Sun (Neckel and Labs 1984, Labs *et al.* 1987). The comet's spectrum is the same as the solar spectrum plus fluorescence emission lines and any reddening of the dust. Using CCD imaging taken on 12 Oct 1996 UT with the Lowell Observatory 1.1-m Hall telescope and narrow-band International Halley Watch filters (as described by Vanýsek [1984]), we found the dust to be at most only 0.03 ± 0.05 mag redder than the Sun. Moreover we found that CN and C_2 emission (the dominant species in Team 5's spectral range) would contribute only about $6\% \pm 1\%$ of the flux. Hence the solar spectrum in Fig. 4.2 is actually a good representation of the comet's spectrum. In Oct 1996 the comet had almost constant morphology and magnitude, so there is little error in using images taken 7 days after the occultation.

Thus we can calculate the relative star and comet brightnesses to within a few

Figure 4.1 (next page): Locations of observers for occultation by Hale-Bopp. Here is a map of the western United States showing the locations of the participating teams (crossed-squares) and the occultation track predictions. The long-dashed lines show the original ephemeris prediction; short-dashed lines show intermediate solution including astrometric corrections; solid lines show last prediction including corrections from deriving the nucleus' position within the comet's photocenter. The three lines mark out a 200-km wide swath, which was used for planning purposes; the nucleus' shadow is much narrower.

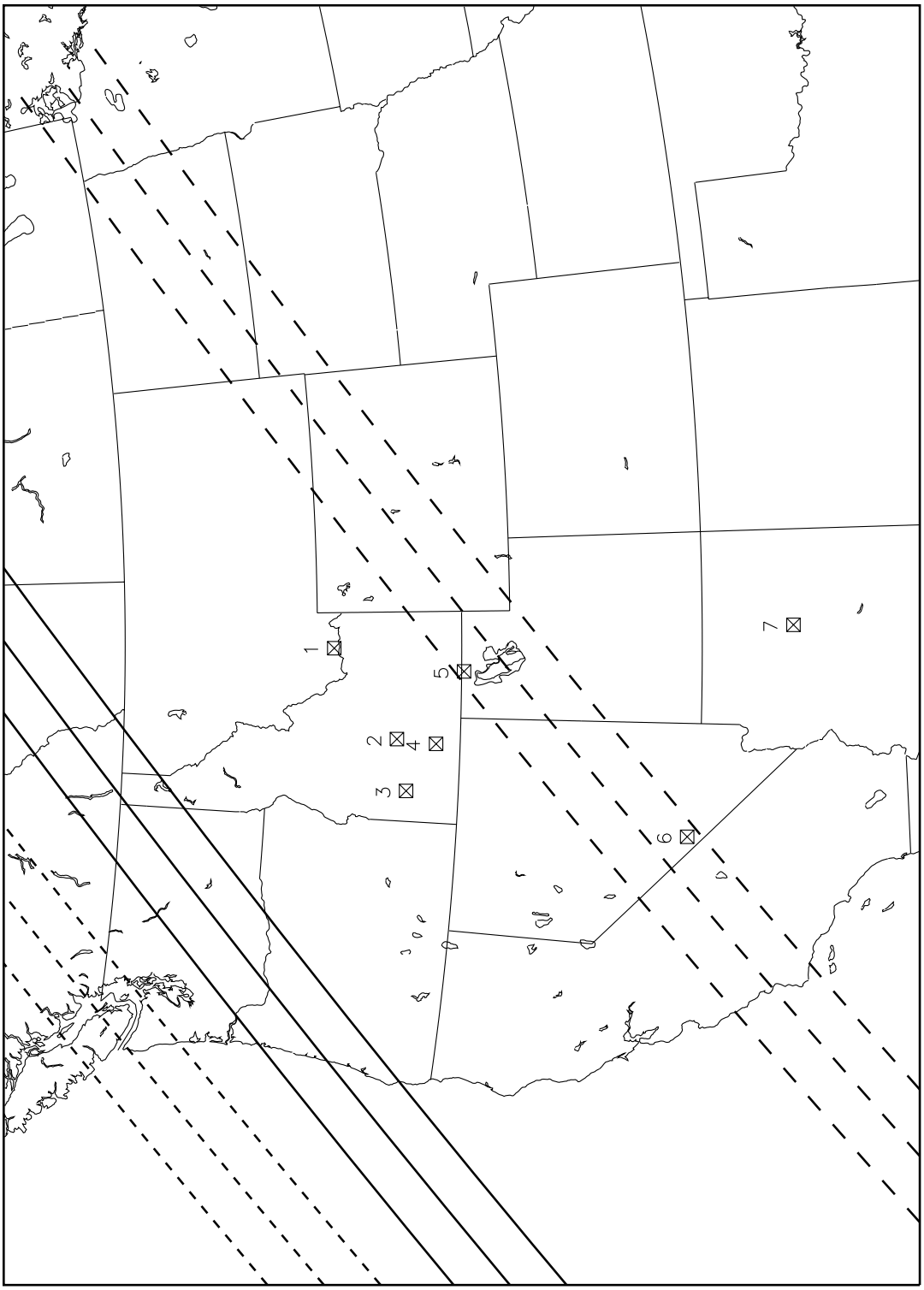
1
2
3
4
5
6
7

percent. The only caveat is that the systematic error may be higher if our star is not a typical K0V star. Our remaining task is to account for sky and detector noise contributions. The latter we measured to be negligible compared to that of the sky and the comet. From practice observations in conditions roughly as dark as for the observation of the occultation itself, we found the sky to be about 8%±2% of the comet's brightness, thus the factor from the spectral analysis should be divided by 1.08 ± 0.02. The combination of all information yields $C = 0.35 \pm 0.02$.

4.2.3 Data

The light curve from Team 5 is shown in Fig. 4.3. The data span about 34 minutes (top graph); the ∼7 minutes centered on the time of deepest occultation (at 03:17:48 UT ±3 s) are shown in the lower panel. The photometer integrations were 100 ms long, and the aperture was circular and one arcminute wide.

The light curve is characterized by (a) long (several minute), gradual changes in the count rate due to passing clouds (e.g., the general trend from 03:14:30 to 03:27:30); (b) precipitous drops in flux due to the comet and star (which were nearly superimposed) being near the edge of the aperture, immediately followed by even more rapid (few second) rises as the target is restored to the center of the field of view (e.g., at 03:26 and 03:27:45); (c) small drops in flux due to the comet and star moving a bit off-center in the aperture, followed by a quick restoration as the target is recentered (e.g., at 03:11:30, 03:16:30, 03:19:00, 03:20:00 and [importantly] at 03:17:35); and (d) the occultation event itself near 03:17:48. The distinct morphological differences between these four types give us confidence that we have observed the occultation event. The occultation caused a fairly symmetric valley in the light curve of about one minute in length, shorter than the time scale for the effects of passing clouds, but longer than the time scale for a drop and rise in flux due to the position of the target in the aperture.

Cases (b) and (c) above were caused by the telescope not exactly tracking at the proper motion rate of the comet. The times of these corrections are marked with arrows in Fig. 4.3. The correction at 03:17:35, the one before it, and the two after were all minor and belong to case (c). Since most of the comet's flux was in its coma, a slight offset of the target did not cause a significant decrease in flux; the more obvious manifestations of these corrections are the small noise spikes from the telescope drive's electrical interference.

The drop in count rate at the time of deepest occultation is about 25%, which is consistent with the star being totally blocked from view, since it was 0.35 times the brightness of the other contributors to the flux ($0.35/1.35 \approx 25\%$). Moreover it occurs close to the predicted time of 03:18:10 for the location of Team 5. The dip could not be due to a jet contrail since the light curve would resemble a profile through a uniform density gas cylinder, which would have a shallower slope through the middle of the event, unlike what has been recorded. While we cannot unambiguously rule out that an unusual cloud passed in front of the comet, the circumstantial evidence does imply an observation of the occultation.

There is a dip in the light curve at approximately 03:12:30 UT which may be interpreted as morphologically distinct from the effects of both clouds and tracking errors, and so could be construed to be the occultation event; it is the only other

Figure 4.2 (next page): Comparison of occulter (cometary) and occultee (stellar) spectra. The dashed lines give the bandpass of the observing system at the USNO 1.5-m telescope and of the C-14 and photometer system used by Team 5 for the occultation. A comparison of the spectra (solid lines) of a K0V star and a solar-type star, which in this case approximates the spectrum of the comet, was used to transform the relative brightnesses of the comet and star from the USNO system to the Team 5 system.

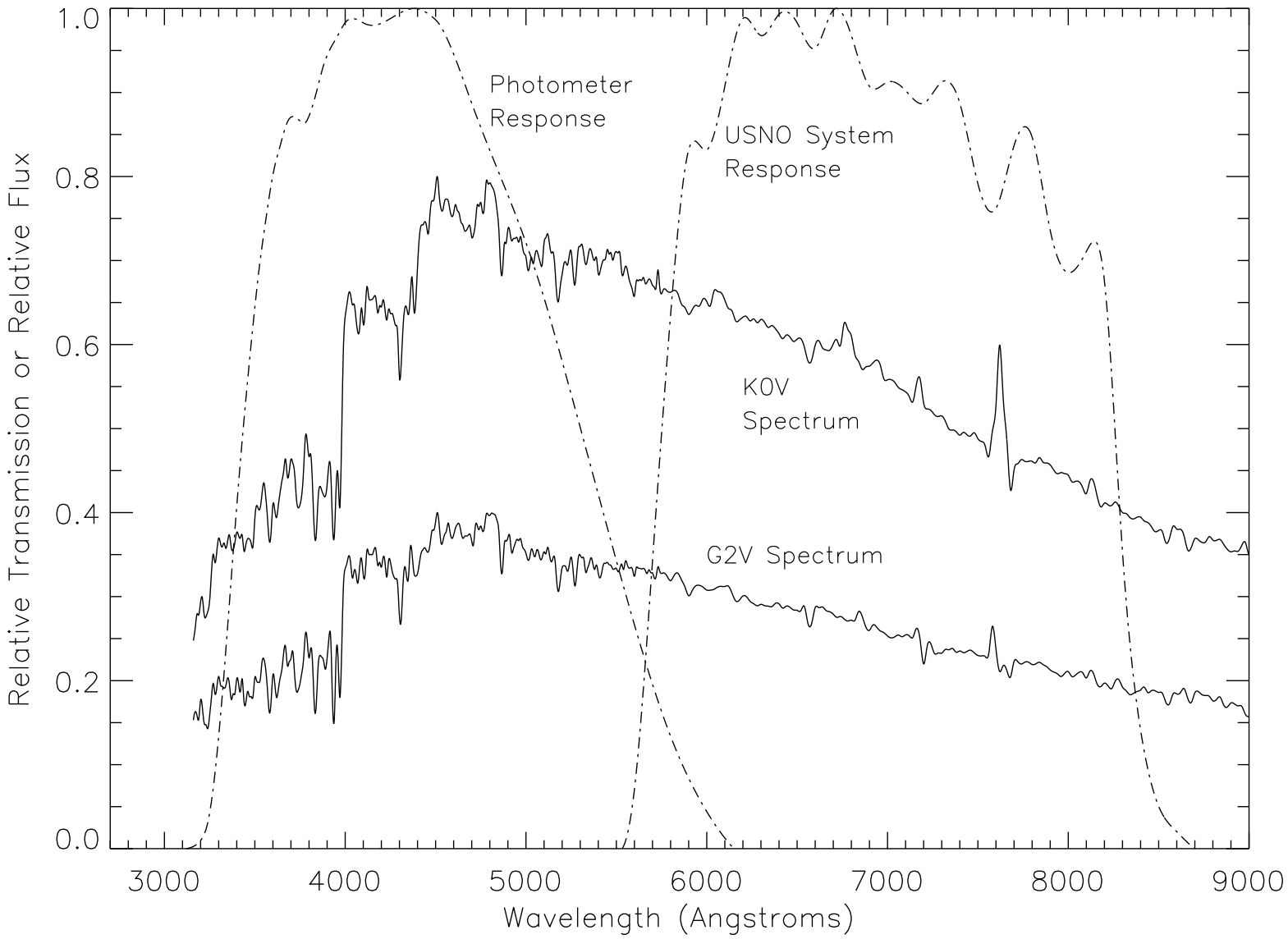
Photometer
Response
USNO System
Response
K0V
Spectrum
G2V Spectrum
Relative Transmission or Relative Flux
Wavelength (Angstroms)
0.0
0.2
0.4
0.6
0.8
1.0
3000
4000
5000
6000
7000
8000
9000

Figure 4.3 (next page): Light curve of occultation by Hale-Bopp, Team 5. This light curve shows the occultation event, a feature that is morphologically distinct from all others. The top plot covers all 34 minutes of the light curve; bottom plot shows 7 minutes centered on the occultation feature. The integration time for each data point was 100 ms. Arrows indicate tracking corrections; see text for details. The tracking correction near the center of the occultation was not significant. The asterisks indicate the locations where the large-scale effect of the cirrus clouds was sampled, and the thick line is a spline fit to those points. This fit was used by our model to grossly account for the non-photometric conditions.

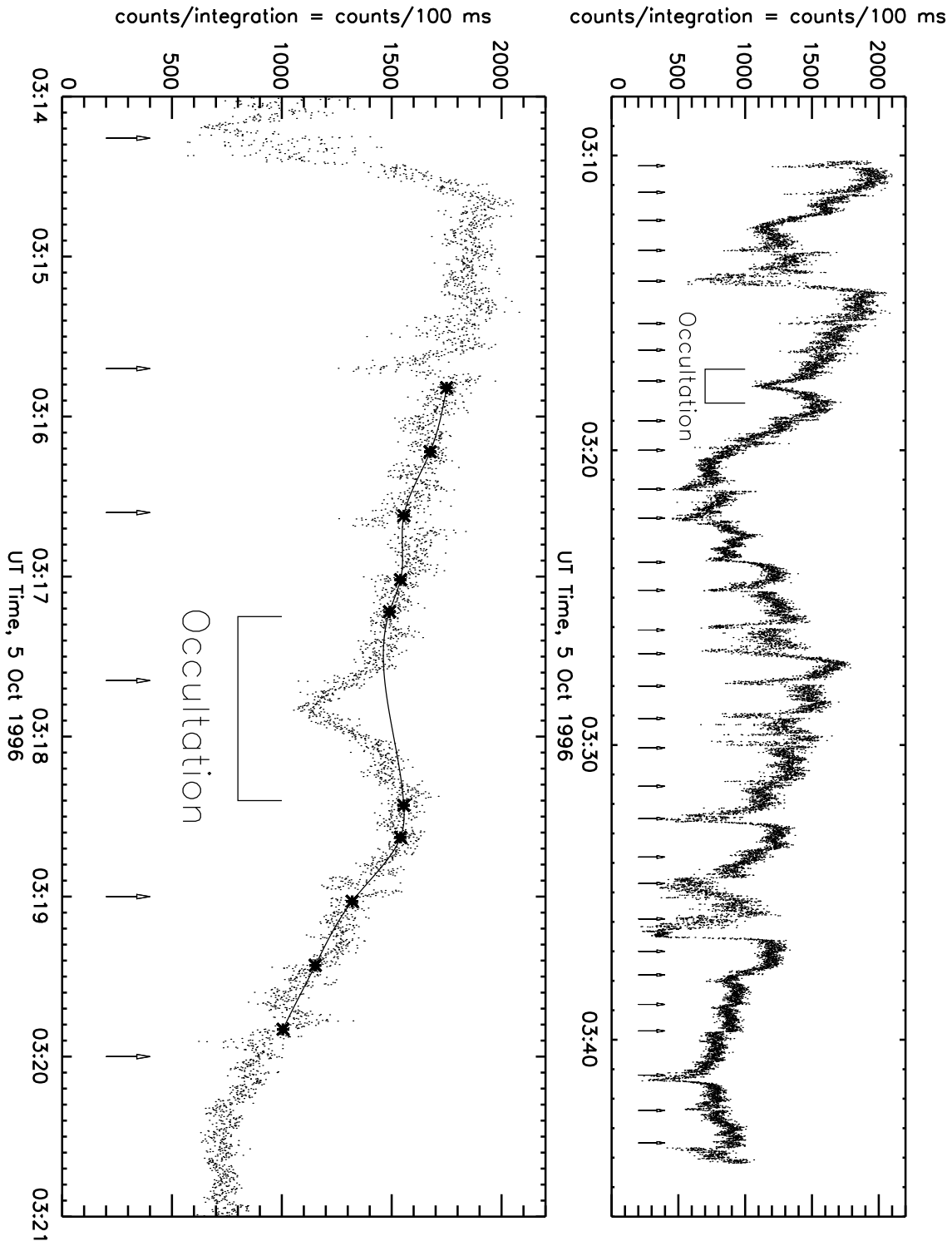
counts/integration = counts/100 ms
0
500
1000
1500
2000
Occultation
03:10
03:20
03:30
03:40
UT Time, 5 Oct 1996
counts/integration = counts/100 ms
0
500
1000
1500
2000
Occultation
03:14
03:15
03:16
03:17
03:18
03:19
03:20
03:21
UT Time, 5 Oct 1996

feature in the light curve, aside from the one at 03:17:48 UT, that could have been caused by the occultation. An event this early would, however, imply a rather large error of thousands of kilometers. While it is possible to model the circumstances of the event (in the manner described in the next section) to reproduce the curve, the fits are less robust than those for the 03:17:48 feature. Accounting for the effects of extinction by the clouds makes the feature quite skew, which reduces the ability of our model to adequately fit it.

In sum, due to the unique shape of the feature at 03:17:48, our ability to model it well, its closeness to the predicted time, and its depth, we believe that it is likely due to the occultation event and not due to tracking errors or clouds.

The light curve recorded by Team 6 is shown in the top of Fig. 4.4, observed from a position 643 km farther along the shadow track from Team 5, and 170 km perpendicular to it. This light curve was obtained in a cloudless sky so all variations are due to tracking errors, gain changes, and manifestations of the occultation. At the time one would expect the comet's shadow to pass over Team 6 (based on Team 5's results; marked on the figure), there is a drop in flux of a few percent (lower panel of Fig. 4.4). That feature's shape is similar to other tracking error corrections in the light curve, so it is not clear if this is the occultation. However, it does allow us to limit the opacity of the coma 170 km from Team 5's chord at 8%.

4.2.4 Analysis

4.2.4.1 Model and Assumptions

Our model for the light curve assumes the optical depth, τ, is proportional to the inverse of the cometocentric distance, $1/\rho$, raised to a constant power n. (The steady-state, force-free, radially-flowing dust coma would have $n = 1$.) As the comet passes between Earth and the star, the attenuation of starlight will depend on time. A schematic of the scenario is given in Fig. 4.5. Ignoring clouds for the moment, we express each point in the light curve, $S(t)$, as a constant term (S_0, the comet's flux plus sky flux and detector noise) plus a term representing the star's flux times the attenuation factor ($e^{-\tau(t)}$). Let $C = 0.35 \pm 0.02$ be the ratio of the star's unattenuated flux to S_0. Then $S(t) = S_0(1 + Ce^{-\tau(t)})$. If the comet's nucleus itself passes between the star and Earth, the flux during that interval will just be S_0. If the star disappears behind the nucleus at time t_i, and reappears at time t_o, then the light curve can be represented by

$$S(t) = \begin{cases} S_0(1 + Ce^{-\tau_i(t)}), & \text{if } t < t_i; \\ S_0, & \text{if } t_i < t < t_o; \text{ and} \\ S_0, (1 + Ce^{-\tau_o(t)}), & \text{if } t > t_o. \end{cases} \tag{4.1}$$

Since we do not assume *a priori* that the two sides of the coma that are sampled by the inbound and outbound sections of the occultation are the same, we have a three-piece function. We can however remove the nuclear chord in the model simply

Figure 4.4 (next page): Light curve of occultation by Hale-Bopp, Team 6. This light curve has the expected time of the occultation marked, based on the time of deepest occultation recorded by Team 5. The Top panel shows the whole curve; lower panel shows a close-up of the most relevant section. Ordinate units are arbitrary. There is a slight dip in the count rate at the appropriate time, but it is not distinguishable from other, comparably-shaped features.

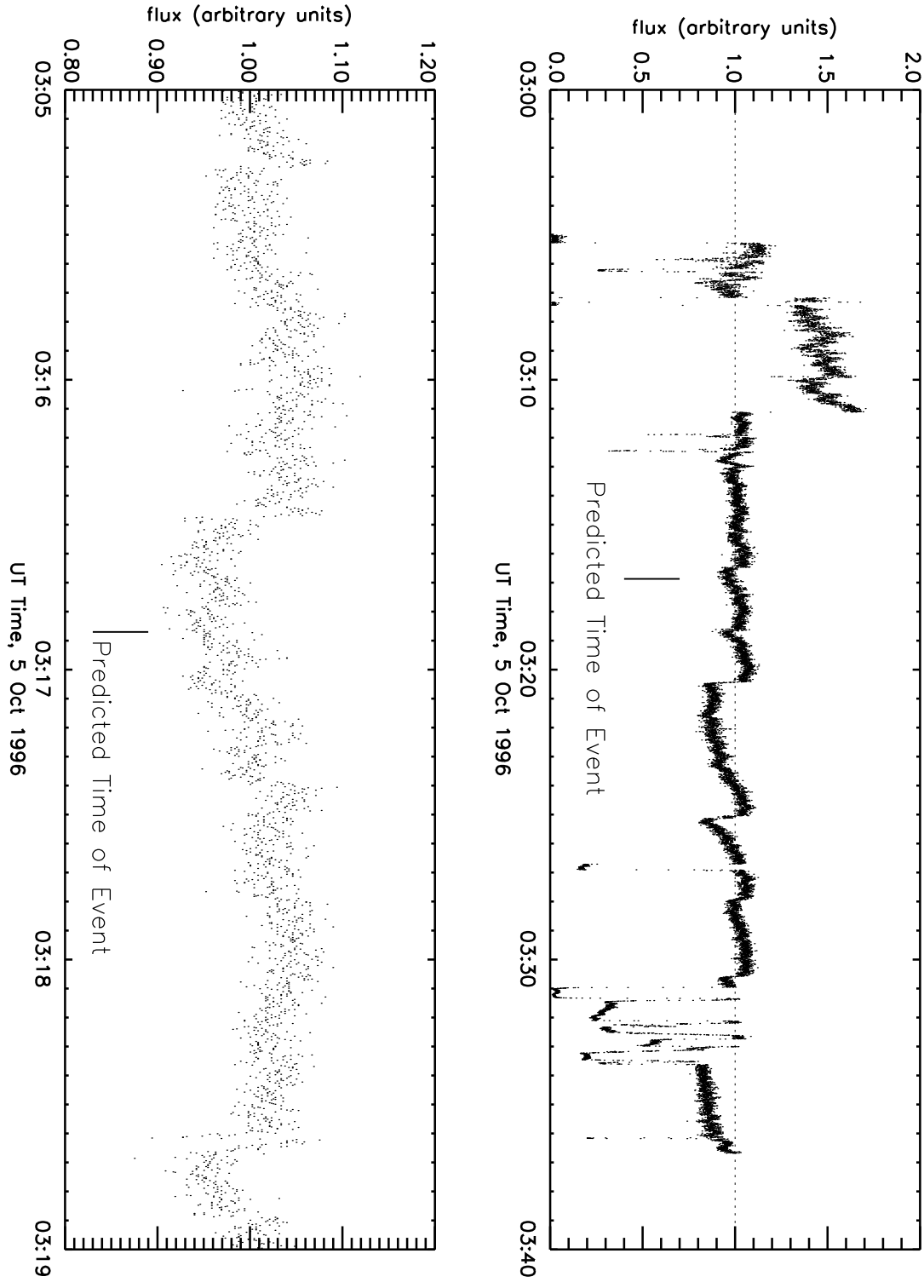
flux (arbitrary units)
2.0
1.5
1.0
0.5
0.0
03:00
03:10
03:20
03:30
03:40
UT Time, 5 Oct 1996
Predicted Time of Event
flux (arbitrary units)
1.20
1.10
1.00
0.90
0.80
03:05
03:16
03:17
03:18
03:19
UT Time, 5 Oct 1996
Predicted Time of Event

by setting $t_i = t_o$. The subscript i denotes a quantity related to the ingress; o, to the egress.

Evaluating τ as a function of time requires knowing ρ. The distance from the center of the nucleus at a given time t is just $\sqrt{b^2 + (v(t - t_m))^2}$, where b is the impact parameter, v is the speed of the comet across the sky, and t_m is the time of mid-occultation. Since the center of the (assumed spherical) nucleus does not have to be the coordinate origin for ρ, we include an extra term, l_0, that describes the offset (parallel to the star's direction of motion) of the coordinate origin from the nuclear center. Thus, $\rho(t) = \sqrt{b^2 + (v(t - t_m) - l_0)^2}$ and the optical depth is given by

$$\tau_i(t) = \left(\frac{\kappa_i}{\sqrt{b^2 + (v(t - t_m) - l_{0i})^2}} \right)^{n_i}, \tag{4.2a}$$

$$\tau_o(t) = \left(\frac{\kappa_o}{\sqrt{b^2 + (v(t - t_m) - l_{0o})^2}} \right)^{n_o}, \tag{4.2b}$$

where κ is the length scale of the opacity. Since we allow the time t_m to be fit by the model, we have overparameterized the lateral shift in the coordinate origin; the best parameter to quote really is $\Sigma l_0 \equiv l_{0i} + l_{0o}$, i.e., the separation of the two coordinate origins. In later discussion we will mention the nuclear radius, R, which is just

$$R = \sqrt{b^2 + (\frac{1}{2} l_n)^2} \equiv \sqrt{b^2 + \left(\frac{1}{2} v(t_o - t_i)\right)^2}, \tag{4.3}$$

i.e., the square root of the quadrature-addition of the impact parameter and half the length of the chord through the nucleus. A listing of all quantities is given in Table 4.3.

Note that the impact parameter b was *not* used as a measure of the offset from the coordinate origin in the perpendicular direction. The coordinate origin always lies on the horizontal line in Fig. 4.5 that runs through the center of the nucleus. There is no evidence that our assumption is justified but it does make the modeling tractable and allowed us to constrain properties of the nucleus.

In addition to this theoretical model, we accounted for the large-scale extinction in the light curve due to clouds near the time of the event by multiplying our model by an empirical function. On Fig. 4.3, the asterisks in the light curve indicate where it was sampled to estimate the clouds' effect. The thick line is a spline fit through those points and represents the empirical function. We sampled the clouds' effect outside the region to which we applied our model. The observation site of Team 5 was dark and moonless, so the clouds would only cause extinction of the starlight, not increase the sky brightness.

We have made some assumptions to simplify the fitting. The spherical nucleus assumption immediately implies that $t_o - t_m = t_m - t_i$. Also note that our model coma (Fig. 4.5) is not perfectly circular; n and κ can be different between the two hemispheres, but within one hemisphere they cannot vary. We have not included in our fitting the data near the time of the tracking correction (2.8 seconds centered at 03:17:45.9 UT), and two brief noise spikes (0.5 seconds starting at 03:17:39.0 UT;

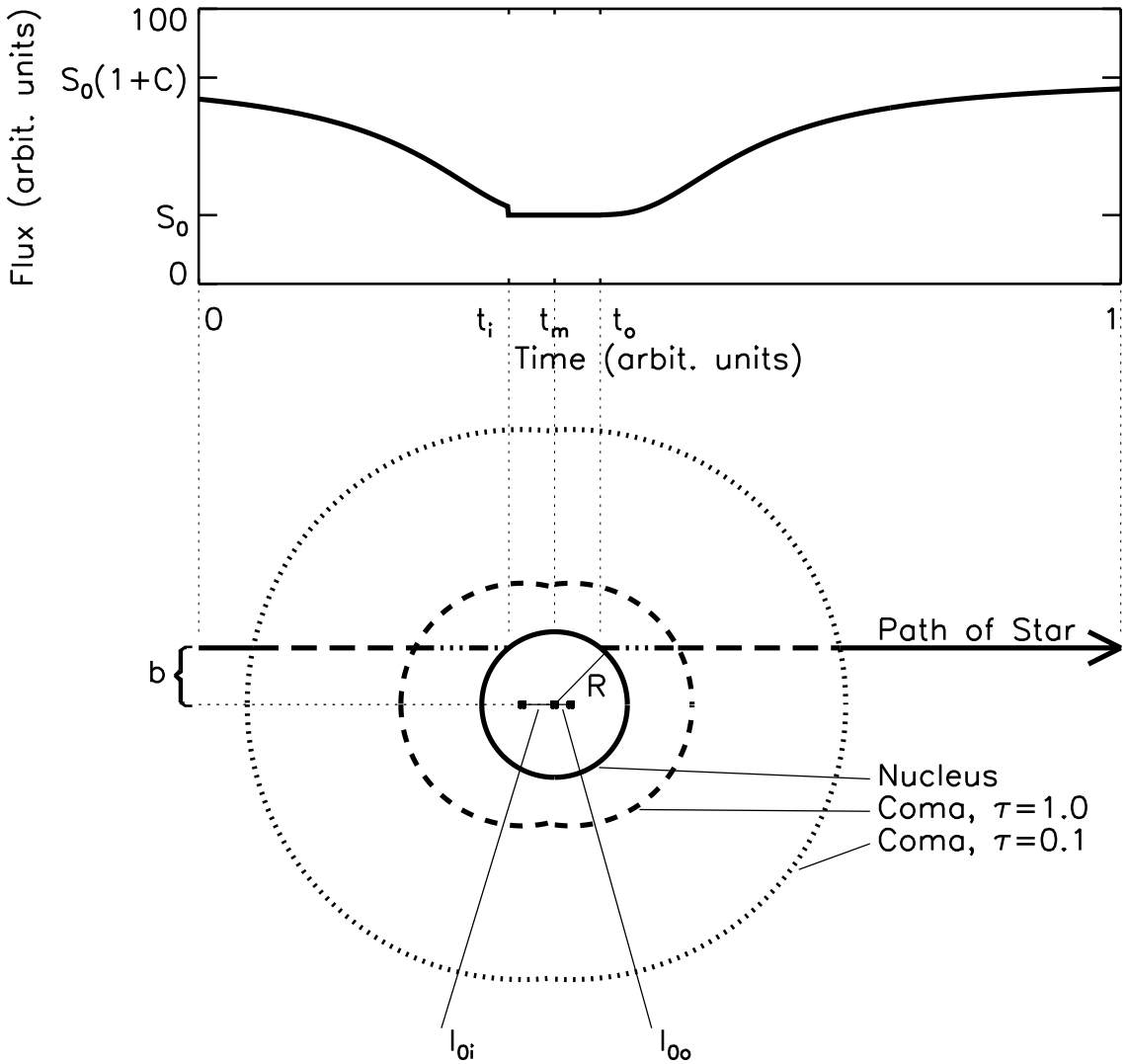

Figure 4.5: Schematic of occultation scenario and light curve. The top plot shows a generic light curve based on the star's passage behind the coma and nucleus of the comet. The arrow in the drawing indicates the star's motion. Times of the beginning and end of nuclear chord are marked (t_i and t_o, respectively), as is mid-occultation (t_m); note the abrupt jump in the flux at time t_i as the star passes behind the nucleus. The locations of a coma opacity of 0.1 and 1.0 are marked. All variables are defined in Table 4.3.

Table 4.3. Parameters of the Model of Nuclear and Comatic Structure

Symbol	Description
Fit Variables	
S_0	count rate from comet+sky+dark current
t_i & t_o	beginning and ending times of occultation by nucleus
t_m	time of mid-event
l_n	length of the nuclear chord of the occultation
b	impact parameter
n_i & n_o	exponent of the power-law profile of the opacity
κ_i & κ_o	length scale of the opacity
l_{0i} & l_{0o}	distance of cometocentric coordinate origin from center of nucleus
Variables Derived from Fit	
τ_i & τ_o	opacity
R	nuclear radius
Known Constants	
C	ratio of count rate from star to S_0 (0.35 ± 0.02)
v	speed of comet across sky (5.11 km/s)
Subscripts	
subscript i & o	variable pertains to ingress and egress of occultation

1.3 seconds starting at 03:17:52.8 UT; see Fig. 4.3). Lastly, we have assumed that the radius of the nucleus is no bigger than 50 km. Analysis of high-resolution mid-infrared, microwave, and optical imaging of the comet have constrained the nuclear size to be smaller than this value (Altenhoff *et al.* 1999, Weaver and Lamy 1999, and a later section of this Chapter), so our assumption allows for a large error in these works. In terms of our fitting, this means we will not consider models that require a combination of b and l_n such that $R \geq 50$ km.

Further assumptions were made about the physical environment of the coma. First, we assumed that n could be no larger than 2.4. Hydrodynamic models of the coma (Divine 1981) imply that a steepening of the dust density profile to the equivalent of ρ^{-3} (yielding a surface brightness (and opacity) proportional to ρ^{-2}) can occur within a few nuclear radii of the nucleus. Others (e.g., Gombosi *et al.* [1983, 1985], Marconi and Mendis [1983, 1984]) have also used dusty-hydrodynamic models to calculate dust velocities and/or number densities as a function of cometocentric distance, and their results do show some steepening of the dust profile within a few nuclear radii of the surface. From these works we conjecture that the tenable limit to n in this phenomenon is ~ 2 to $2\frac{1}{2}$, though the higher values have less theoretical support. Again, we allow for a large error in these previous works. Our second assumption is that l_0 can not be so large as to extend off the near edge of the nucleus itself. In other words, we did not allow the case where $\rho = 0$ (and the divergence of the opacity) could be encountered by the star.

4.2.4.2 Results of Model Fitting

Since there are so many data points, in this case the χ^2 statistic is useful only as a coarse indicator of "good" and "bad" fits; e.g., a fit that goes through all of the points but is too shallow to cover the light curve's minimum could have a reduced χ^2 (χ^2_R) of just 1.15, which would still be beyond the 99% confidence level for the 620-odd degrees of freedom. The best way to ascribe a "good" fit is by eye, with χ^2 being a rough guide. There are three morphological characteristics that must be satisfied for a fit to be considered "good": a) it must be sufficiently deep to cover the valley at 03:17:48 UT (determined by κ, n, b, and to some extent by $t_o - t_i$); b) it must follow the shape of the valley's walls (from 03:17:33 to 03:17:45 and from 03:17:53 to 03:18:03 UT; determined by κ, n, and l_0); and c) it must lie on the median value of the wings (from 03:17:15 to 03:17:33 and from 03:18:03 to 03:18:22 UT; determined by κ and n). We say "median" because we do not attempt to fit the small jumps in flux that occur in the wings; these may be due to clouds or to real opacity features in the comet's coma. A given model was detuned with the various parameters until the fit could no longer be considered marginally "good."

The results of the fitting are summarized in Table 4.4. We have explored parameter space using $b = 0, 6.5, 11, 22, 26, 33, 39$, and 45 km (and higher values, but it turned out that they never sufficiently fit the light curve), and $n = 0.8$, 1.0, 1.2, 1.4, 1.6, 1.8, 2.0, and 2.4. Entries in the table give values or ranges for the quantities κ_i, κ_o, and l_n that yield "good" or marginally "good" fits as defined above. (In the "Comments" column, the presence or absence of "m" indicates a marginally good or good fit.) All fits listed in the table have $0.96 \leq \chi^2_R \leq 1.05$, with most around 0.97, 0.98, or 0.99. With only one chord through the comet showing unambiguous

extinction, the valid parameter space offered by our model is large. Moreover, the unfortunate location of the tracking correction so close to the valley of the light curve, thus removing those data points, allows an even wider valid space.

Figure 4.6 displays representative fits to our light curve. It is not meant to be as exhaustive as Table 4.4 is, but graphically shows the large variation in parameter values that still allows adequate fitting. The first four plots have forced $\Sigma l_0 = 0$, the last four allow it to vary. The value of b is written within each plot. The abrupt jumps in the flux predicted by some models are due to the star passing behind the nucleus; note the jump at time t_i in the schematic light curve of Fig. 4.5. Special note should be taken of one model in Fig. 4.6a using $n_i = n_o = 1.0$; it cannot fit the curve. Also, Fig. 4.6d shows a model with $b = 39$ km; such a high impact parameter allows only a marginal fit to the curve. The value of χ^2_R is 1.0 in all but the one obviously incorrect model, where it is 1.2.

We mention some other notable results from the modeling:

• Our modeled constraints on b limit the nucleus' radius R (via Eq. 4.3) to ≤ 48 km. Restricting ourselves to the best (not marginal) fits and to $n \leq 2.0$, then $R \leq 30$ km.

• For completeness we modeled the case where $b = 0$ and $l_n = 0$, even though clearly this is an unphysical scenario. Fortunately, it was never the case that the light curve was significantly better fit with $l_n = 0$ than with $l_n > 0$.

• The distance from the coordinate origin to the $\tau = 1$ point in the coma is given by κ. For some models in Table 4.4 $R > \kappa$, so the maximum coma opacity is less than unity. (The fit to the light curve for these models requires the nuclear chord to pass through the bad-data gaps.) On the other hand with a small R the maximum opacity can be as high as 2. Note that the noise in the light curve prevents us from confidently distinguishing between $\tau = 2$ and $\tau > 2$ (or $\tau = \infty$).

• For clarity we have not put in the allowable ranges of κ for each model in Table 4.4. Typically changing κ by ± 3 km still yields a good or marginally good fit.

• The acceptable fits to the light curve require n to be at least 1.0, though the fits are slightly better as n increases. Further, if $n \leq 1.2$ in one hemisphere, then $n \geq 2.0$ in the other. This steepness to the coma is opposite the sense found in *Giotto* images of comet Halley's inner coma, where $n < 1$ as $\rho \to R$ due to localized sources of dust on the surface (Thomas and Keller 1990, Reitsema *et al.* 1989). We postulate that the steepness in Hale-Bopp's coma is due to azimuthal structure (where we have assumed none) and/or to the passage of the star's path through the acceleration region of the dust. Clearly our model is simplistic, but the lack of data does not justify using a more complex formulation.

• One power law can satisfy the constraints of the light curves measured by both Team 5 and Team 6 if, in general, $n \geq 1.6$. A letter "c" in the "Comments" column of Table 4.4 indicate which models are consistent with both curves. Furthermore, if we force the coma to be consistent, it would then be impossible for the nuclear shadow to have passed between the two teams. I.e., if Teams 5 and 6 were on opposite sides of the nucleus, the parameters describing the two sides of the coma sampled by the two teams would have to be different, which is beyond the scope of our modeling. An alternate explanation is that the coma merely does not have the spherical or hemispherical symmetry that is assumed.

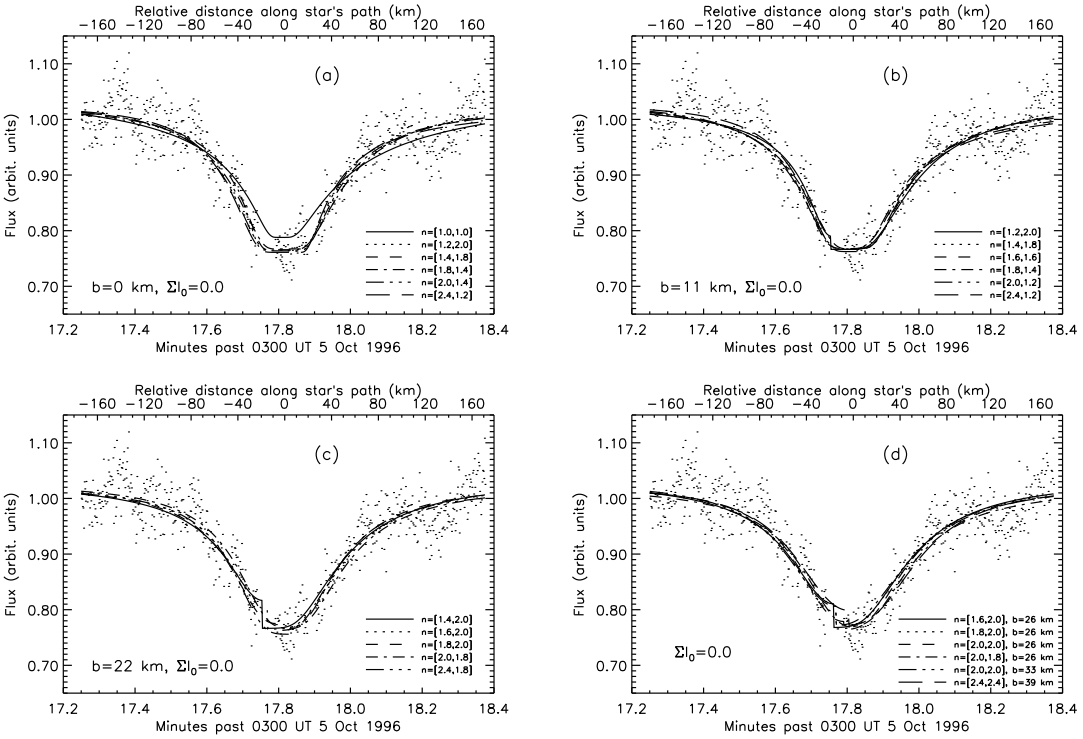

Figure 4.6a-d: Example model fits to occultation light curve. Shown here are example "good" model fits using various combinations of parameters, overlaid on the Team 5 light curve. This is not an exhaustive portrayal of the entire valid parameter space, but only demonstrates how well the curve can be fit. All models presented here assume there was no nuclear chord. Each plot has the impact parameter b written within its borders. The first 4 plots assume $\Sigma l_0 \equiv l_{0i} + l_{0o} = 0.0$. Each plot shows 5 or 6 models with varying n_i and n_o (written as $n = [n_i, n_o]$). Plot (a) shows clearly that $n_i = n_o = 1.0$ does not fit the curve; plot (d) shows an example of an impact parameter higher than ~ 35 km that marginally fits the curve. The blank section near 17.7 minutes past 0300 UT, caused by a tracking correction, allows for great latitude in the kind of models that can fit the data.

• For most models, we find -10 km $\leq \Sigma l_0 \leq 15$ km, though for $b > 30$ km, the range is only a few kilometers. Moreover, having the coordinate origin of both hemispheres on the ingress side of the nucleus is slightly favored (by a $\leq 2\%$ decrease in χ^2_R). Note that in comet Halley, the origin was found to be near the center of the nucleus (Thomas and Keller 1987).

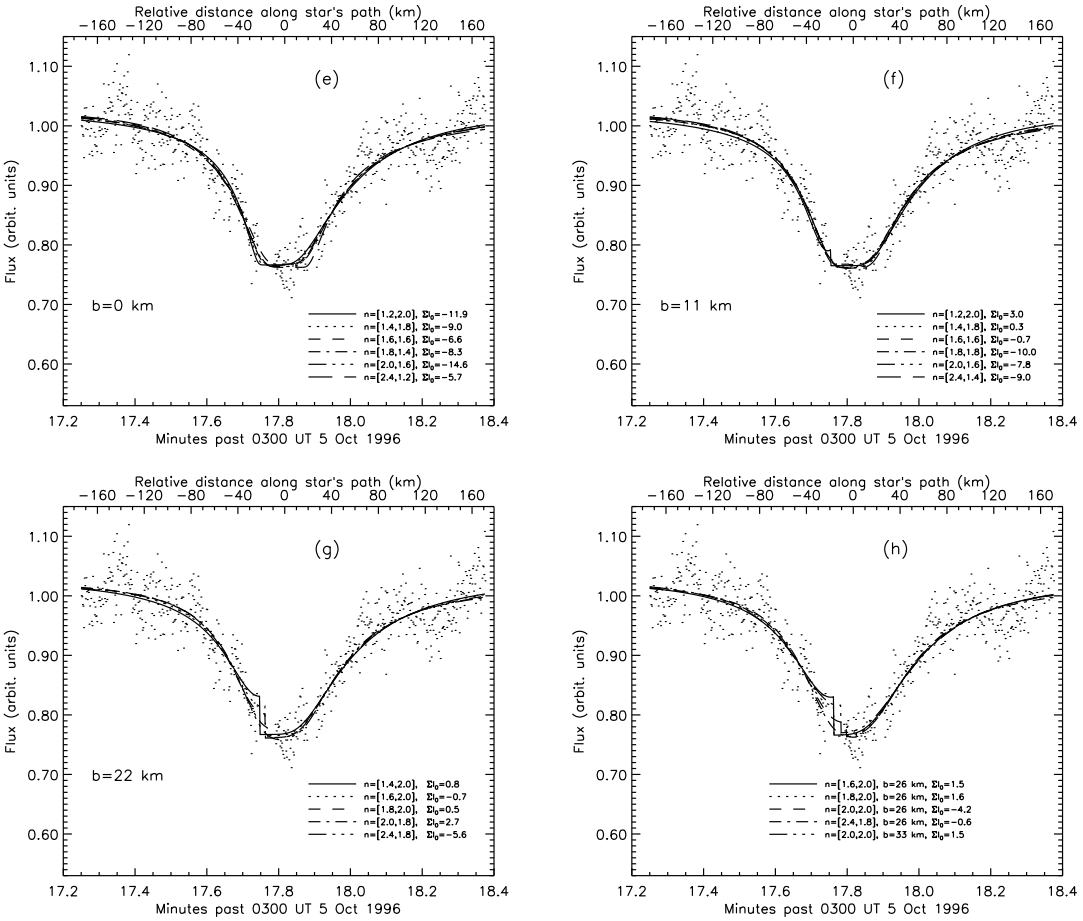

Figure 4.6e-h: Example model fits to occultation light curve. Here is the same scenario as for 6a-d, except the 4 plots allow $\Sigma l_0 \neq 0.0$, and each model mentions the value used.

Table 4.4 Constraints on Parameters to Occultation Model

b (km)	n_i	n_o	κ_i (km)[a]	κ_o (km)[a]	$\rho(\tau = 0.1)$ [b]	$\overline{1 - e^{-\tau}}$ [c]	l_n range (km)[d]	R range (km)[e]	Comm. [f]
0	1.0	1.8	21	64	[157,188]	0.40	0-26	0-13	m
0	1.0	2.0	19	66	[155,190]	0.39	0-22	0-11	
0	1.0	2.4	16	67	[153,174]	0.36	0-15	0-8	
0	1.2	1.8	25	61	[159,185]	0.41	0-24	0-12	m
0	1.2	2.0	23	60	[159,185]	0.38	0-24	0-12	
0	1.2	2.4	20	62	[135,159]	0.35	0-24	0-12	m, c
0	1.4	1.6	32	53	[166,179]	0.44	0-40	0-20	m
0	1.4	1.8	32	54	[162,179]	0.42	0-40	0-20	
0	1.4	2.0	28	55	[143,175]	0.38	0-36	0-18	c
0	1.6	1.2	45	40	[179,166]	0.48	0-52	0-26	m
0	1.6	1.4	43	44	[177,168]	0.47	0-56	0-28	
0	1.6	1.6	38	47	[158,172]	0.44	0-55	0-23	m
0	1.8	1.2	50	37	[179,161]	0.48	0-42	0-21	m
0	1.8	1.4	43	42	[154,168]	0.46	0-45	0-23	
0	1.8	1.6	42	42	[149,168]	0.43	0-54	0-27	m, c
0	2.0	1.0	54	30	[172,157]	0.49	0-30	0-15	m
0	2.0	1.2	52	34	[164,159]	0.48	0-34	0-17	c
0	2.0	1.4	45	39	[142,166]	0.45	0-48	0-24	c
0	2.0	1.6	44	39	[137,166]	0.43	0-48	0-24	m, c
0	2.4	1.0	55	27	[142,157]	0.48	0-25	0-13	m, c

Table 4.4 – *Continued*

b (km)	n_i	n_o	κ_i (km)[a]	κ_o (km)[a]	$\rho(\tau = 0.1)$ [b]	$\overline{1 - e^{-\tau}}$ [c]	l_n range (km)[d]	R range (km)[e]	Comm. [f]
0	2.4	1.2	53	29	[140,157]	0.46	0-27	0-14	m, c
0	2.4	1.4	52	30	[135,154]	0.44	0-30	0-15	m, c
6.5	1.0	1.8	22	67	[155,190]	0.39	0-15	0-10	m
6.5	1.0	2.0	19	68	[153,192]	0.37	0-15	0-10	
6.5	1.2	1.6	26	60	[160,186]	0.40	0-28	0-15	m
6.5	1.2	1.8	26	61	[160,186]	0.39	0-25	0-14	
6.5	1.2	2.0	23	63	[155,188]	0.36	0-25	0-14	m
6.5	1.4	1.4	37	50	[170,175]	0.43	0-47	0-24	m
6.5	1.4	1.6	34	53	[168,177]	0.42	0-46	0-24	
6.5	1.4	1.8	32	55	[163,179]	0.39	0-41	0-22	
6.5	1.4	2.0	27	57	[137,181]	0.36	0-36	0-19	m, c
6.5	1.6	1.4	43	44	[177,168]	0.44	0-55	0-28	m
6.5	1.6	1.6	38	48	[161,172]	0.41	0-54	0-28	
6.5	1.6	1.8	35	50	[147,175]	0.39	0-46	0-24	m
6.5	1.8	1.0	56	33	[188,158]	0.49	0-33	0-18	m
6.5	1.8	1.2	52	35	[185,160]	0.41	0-35	0-19	
6.5	1.8	1.4	47	39	[167,163]	0.36	0-45	0-23	c
6.5	1.8	1.6	42	43	[150,168]	0.31	0-48	0-25	m, c
6.5	1.8	1.8	39	45	[139,159]	0.27	0-54	0-28	m, c
6.5	2.0	0.8	64	23	[196,149]	0.49	0-15	0-10	m

Table 4.4 – *Continued*

b (km)	n_i	n_o	κ_i (km)[a]	κ_o (km)[a]	$\rho(\tau = 0.1)$ [b]	$\overline{1 - e^{-\tau}}$ [c]	l_n range (km)[d]	R range (km)[e]	Comm. [f]
6.5	2.0	1.0	60	26	[190,151]	0.45	0-18	0-11	
6.5	2.0	1.2	53	32	[168,158]	0.40	0-33	0-18	m, c
6.5	2.4	0.8	64	20	[166,148]	0.47	0-15	0-10	m
6.5	2.4	1.0	62	22	[162,149]	0.44	0-13	0-9	m, c
6.5	2.4	1.2	57	26	[148,153]	0.41	0-19	0-12	m, c
11	1.0	1.8	22	70	[153,192]	0.38	0-15	0-13	m
11	1.0	2.0	20	72	[151,194]	0.37	0-11	0-12	
11	1.2	1.8	25	64	[158,188]	0.38	0-23	0-16	m
11	1.2	2.0	23	65	[155,190]	0.36	0-17	0-14	c
11	1.4	1.6	34	55	[166,179]	0.36	0-35	0-21	m
11	1.4	1.8	31	57	[159,182]	0.38	0-30	0-19	c
11	1.4	2.0	28	59	[145,184]	0.35	0-27	0-17	m, c
11	1.6	1.4	41	45	[174,170]	0.42	0-52	0-28	
11	1.6	1.6	32	55	[136,182]	0.39	0-30	0-19	c
11	1.6	1.8	30	56	[124,184]	0.33	0-28	0-18	m, c
11	1.6	2.0	27	58	[112,182]	0.32	0-22	0-16	m, c
11	1.8	1.2	52	36	[186,160]	0.45	0-34	0-20	m
11	1.8	1.4	48	40	[171,164]	0.37	0-39	0-22	
11	1.8	1.6	43	44	[154,168]	0.40	0-48	0-26	m, c
11	2.0	1.2	53	34	[166,160]	0.44	0-33	0-20	c

Table 4.4 – *Continued*

b (km)	n_i	n_o	κ_i (km)[a]	κ_o (km)[a]	$\rho(\tau = 0.1)$ [b]	$\overline{1 - e^{-\tau}}$ [c]	l_n range (km)[d]	R range (km)[e]	Comm. [f]
11	2.0	1.4	49	37	[156,162]	0.37	0-33	0-20	m, c
11	2.0	1.6	47	39	[147,164]	0.33	0-39	0-22	m, c
11	2.4	1.0	58	28	[152,155]	0.46	0-15	0-13	m, c
11	2.4	1.2	55	31	[142,158]	0.43	0-20	0-15	m, c
11	2.4	1.4	53	31	[138,158]	0.38	0-25	0-17	m, c
22	1.4	2.0	30	66	[157,189]	0.34	0-22	0-25	m, c
22	1.4	2.4	26	72	[134,187]	0.32	0-13	0-23	m, c
22	1.6	1.8	33	62	[141,187]	0.36	0-24	0-25	m, c
22	1.6	2.0	33	63	[138,187]	0.34	0-25	0-25	c
22	1.6	2.4	30	65	[126,168]	0.29	0-19	0-24	m, c
22	1.8	1.6	39	55	[138,180]	0.37	0-35	0-28	m, c
22	1.8	1.8	35	58	[124,185]	0.35	0-35	0-28	c
22	1.8	2.0	31	62	[113,189]	0.33	0-25	0-25	c
22	2.0	1.6	47	47	[149,170]	0.38	0-40	0-30	m, c
22	2.0	1.8	38	54	[121,180]	0.35	0-31	0-27	c
22	2.0	2.0	33	60	[105,187]	0.32	0-21	0-24	m, c
22	2.4	1.6	50	41	[131,165]	0.36	0-25	0-25	c
22	2.4	1.8	43	47	[112,169]	0.34	0-35	0-28	c
22	2.4	2.0	39	51	[102,159]	0.31	0-37	0-29	m, c
26	1.6	2.0	33	69	[139,192]	0.35	0-20	0-28	m, c

Table 4.4 – *Continued*

b (km)	n_i	n_o	κ_i (km)[a]	κ_o (km)[a]	$\rho(\tau = 0.1)$ [b]	$\overline{1 - e^{-\tau}}$ [c]	l_n range (km)[d]	R range (km)[e]	Comm. [f]
26	1.6	2.4	30	72	[125,188]	0.32	0-12	0-27	m, c
26	1.8	1.8	40	60	[141,183]	0.36	0-35	0-31	m, c
26	1.8	2.0	34	65	[123,189]	0.33	0-23	0-28	c
26	1.8	2.4	30	70	[107,183]	0.31	0-11	0-27	m, c
26	2.0	1.8	40	59	[124,183]	0.33	0-29	0-30	m, c
26	2.0	2.0	36	62	[113,187]	0.33	0-24	0-29	c
26	2.0	2.4	31	68	[99,176]	0.30	0-15	0-27	m, c
26	2.4	1.8	45	50	[118,174]	0.34	0-45	0-34	c
26	2.4	2.0	42	53	[108,168]	0.32	0-40	0-33	c
26	2.4	2.4	32	65	[82,170]	0.29	0-15	0-27	m, c
33	2.0	2.0	42	65	[132,186]	0.33	0-27	0-36	m, c
33	2.0	2.4	37	70	[118,182]	0.30	0-17	0-34	m, c
33	2.4	2.0	48	56	[124,177]	0.31	10-30	33-36	c
33	2.4	2.4	38	68	[99,177]	0.30	0-15	0-34	c
39	2.4	2.4	50	63	[131,163]	0.28	10-30	39-42	m, c
45	2.4	2.4	59	64	[153,168]	0.28	15-38	46-48	m, c

Table 4.4 – *Notes*

[a] Error from fitting is ±3 km.
[b] Cometocentric distance at which coma opacity is 0.1. Error from fitting is ±20 km. Two values are given, one for each hemisphere.
[c] Mean value of $1 - e^{-\tau}$ within 100 km of nuclear surface. Error from fitting is about 8%.
[d] Range of lengths of nuclear chord that yields an adequate fit. Error from fitting is ±4 km.
[e] Range of possible nuclear radii based on the range of l_n and b.
[f] Comments. Letters' meanings: m = marginally good fit. c = fit is consistent with opacity measured by Team 6.

4.2.5 Discussion

4.2.5.1 Nucleus

As mentioned, we assumed that the nucleus has $R \leq 50$ km, but our fitting further constrains this number, to 30 km, by making two reasonable assumptions. Only marginally good fits are found for models with R much bigger than this, up to 48 km, i.e., almost up to the assumed maximum. For models that yield $R > 48$ km (or even > 50 km, for that matter), the fits are not even marginally "good."

Millimeter wave measurements by Altenhoff *et al.* (1999) and our centimeter wave measurements – as will be seen later in this Chapter – agree with this occultationderived limit. However I emphasize that this occultation analysis assumes a spherical nucleus.

4.2.5.2 Astrometry

Our apparent detection of the occultation implies the nucleus was $(8.0 \pm 0.5) \times 10^2$ km on a perpendicular from the last prediction of the nuclear track. Mid-event occurred about 22 s before the predicted time for the location of Team 5, corresponding to 255 km along the track. Considering the errors involved with the prediction, this is not an unacceptably large offset, as we now explain.

Figure 4.7a shows an image of the comet and star taken one hour before the event (from the USNO Flagstaff Station 1.5-m telescope). Figure 4.7b, showing an expanded view of the central pixels of the comet, is marked with the middle of the brightest pixel ("M"), the location of the centroid of brightness ("C"), and the estimated position of the nucleus using our coma-fitting technique ("L"; ± 0.25 pixel). The pixel size for the images in Fig. 4.7 is 0.33 arcsec (7.2×10^2 km at the comet). Our astrometry of the comet's offset from the ephemeris position (using 3 nights of USNO images, as mentioned in §II) was uncertain to 0.3 arcsec (6.5×10^2 km), i.e., almost one pixel. Combined with the uncertainty from the coma-fitting technique, this gives an 1-σ error of about 7×10^2 km. So it is quite reasonable to expect the nuclear shadow to have passed over a team several hundred kilometers from the predicted center line.

Our constraint on the location of the nucleus is reasonably consistent with 1998 calculations for the orbit of Hale-Bopp (Donald Yeomans, private communication). However, it should be noted that we are estimating the error with respect to the measured position of the comet from the astrometry, not from the ephemeris. Had we used a different ephemeris, say, one that was thought to be more accurate, the only difference would have been to change the offsets measured via the astrometry of the USNO images. We would have arrived at the same prediction and the same observing strategy. Hence, a post-facto ephemeris, which might be used to try to pin down exactly how far Team 5 was from the nucleus' shadow, would not make much difference. In essence, our astrometry provided a truer prediction of the comet's position than any ephemeris would have. Astrometric measurements from post-event imaging would have helped but these data were not taken.

4.2.5.3 Inner Coma: Albedo of Dust Grains

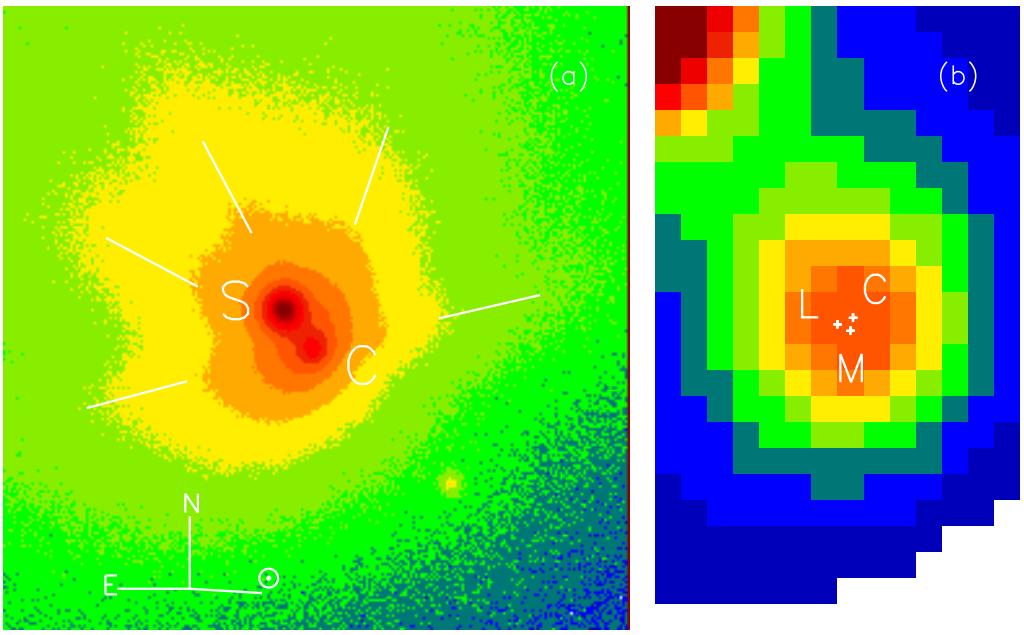

Figure 4.7: Pre-occultation image of comet and star. In (a), an image of both comet Hale-Bopp ("C") and PPM 200723 ("S") is shown, taken less than one hour before the occultation. The scale is 0.33 arcsec per pixel, corresponding to 720 km of linear distance at the comet; our entire occultation event marked in Fig. 4.3 covers about one-half of a pixel. Line segments indicate the most prominent jets in the comet's coma, and show that on ingress the star was traveling along a jet's edge. In (b), I show an expanded view of the central pixels of the comet. The middle of the brightest pixel "M", centroid of brightness "C", inferred position from coma-fitting technique of Lisse *et al.* (1999b) "L".

Since we have measured the opacity of the coma, we can calculate the albedo of the dust in the inner coma by using measured values of $Af\rho_o$, a quantity introduced by A'Hearn *et al.* (1984) where A is the albedo, f is the filling factor, and ρ_o is the size at the comet of the aperture used. It is obtained via

$$Af\rho_o = \frac{F_{\rm comet}}{F_\odot} \times \left(\frac{r}{1{\rm AU}}\right)^2 \times \frac{4\Delta^2}{\rho_o}, \tag{4.4}$$

where r is the heliocentric distance of the comet, Δ is the geocentric distance, $F_\odot$ is the solar flux at Earth, and $F_{\rm comet}$ is the comet's flux measured in the aperture. The filling factor is the aperture-average of $1 - e^{-\tau(\rho)}$. Here the albedo is properly the value of the scattering function relative to a conservative, isotropic scatterer, as outlined by Hanner *et al.* (1981; and equal to $4\pi\sigma(\theta)/G$ in that work).

We analyzed *HST* WFPC2 images of the comet obtained twelve days before and twelve days after the occultation event (provided by H. A. Weaver of Johns Hopkins Univ.), and $Af\rho_o$ was measured down to a cometocentric distance of 400 km (about 0.2 arcsec). A steady-state, force-free, radially-flowing dust coma would have an aperture-independent value of $Af\rho_o$, but since Hale-Bopp's coma was not like this, we extrapolated $Af\rho_o$ down to 100 km for comparison with our occultation results. Since the phase angle of the observations was only 19°, we removed the phase angle effect, $\phi(\alpha)$, by using

$$\phi(\alpha) = 10^{-0.4\alpha\beta}, \tag{4.5}$$

where β is the phase coefficient of 0.025 mag/degree (a value roughly consistent across several comets; Meech and Jewitt 1987), and α is the phase angle at the time of the observation. We estimate that $Af\rho_o/\phi(\alpha)$ was about 1.3 ± 0.3 km on 23 Sep 1996 and 1.9 ± 0.3 km on 17 Oct 1996. Time variability of the comet's flux in the *HST* images leads to the large error estimates. Taking $Af\rho_o/\phi(\alpha) = 1.6 \pm 0.3$ km on 5 Oct 1996, $\rho_o = 100$ km, and the aperture-average of $1 - e^{-\tau}$ to be about 0.38 ± 0.05, we find $A/\phi(\alpha)$ to be 0.04 ± 0.01 (formal error). This leads to an equivalent geometric albedo, p, of $\frac{1}{4}A/\phi(\alpha) = 0.01 \pm 0.002$. (I use the value of $\frac{1}{4}$ to follow the notation of Hanner *et al.* [1981].) This value is rather low (e.g., Divine *et al.* (1986) collate information from various workers to obtain an average p of 0.03 ± 0.01), and a possible explanation (similar to that given by Larson and A'Hearn [1984]) is that a photon is doubly-scattered by the dust in the inner coma. It is not unreasonable to expect such a scenario in the optically-thick portion of the coma. If every photon were doubly-scattered, $A/\phi(\alpha)$ would be the square root of the value given above: 0.21 ± 0.02 (formal error), and $p = 0.05 \pm 0.006$. That the calculated albedo is acceptable provides one self-consistent check that our model results – and specifically the high opacity of the coma – make sense.

4.2.5.4 Inner Coma: Plausiblity of Findings

Our modeling implies that the column density of dust in the inner coma follows a power law of ρ with an index steeper than 1.4. This steepness is not evident in large-scale imaging of the comet. The path of the star's ingress followed the edge of one of Hale-Bopp's jets (short line segments in Fig. 4.7a) that had a surface brightness

proportional to $\rho^{-0.86}$; during egress, the path did not follow a jet, and the coma surface brightness was proportional to $\rho^{-1.26}$. However, one can fit just the wings of our occultation light curve (i.e., between 100 and 170 km from mid-occultation) and match the profiles from the large-scale imaging. It is only in the central region, within 100 km of the nucleus, where these profiles fail and the density of dust must be a steep function of ρ. Unfortunately the small scale of these properties of the coma are beyond the reach of other Earth-based observations – even *HST* Planetary Camera imaging would have covered a full 98 km per pixel.

It is possible that we observed the acceleration region of the dust, and that it may have extended ~ 100 km from the nucleus, steepening the dust profile. Gombosi *et al.* (1986), in their review of inner coma dynamics, state that their modeling shows dust still accelerating toward terminal velocity several nuclear radii away from the nucleus, albeit in a model coma with a lower dust-to-gas ratio (χ) and lower r than Hale-Bopp's. A larger χ could extend the coma's acceleration region, but the larger r (lower insolation, lower dust speed) may counter that effect.

A detailed dusty gas-dynamic model of Hale-Bopp's coma is beyond the scope of this paper, but, using estimates of the dust speed v, we can show the steep opacity profile is roughly compatible with the models of Gombosi *et al.* (1986). We note that azimuthal variations in the dust density (not only the acceleration of the dust) can contribute to the measured shape of the dust profile, but a model of such variations would be difficult to constrain owing to a lack of data. Thus we show here only a gross justification of a steep opacity profile. The profile is proportional to $\rho^{-1.7\pm0.3}$ or so, which makes $v \propto \rho^{0.7\pm0.3}$ (since surface brightness is proportional to $(\rho v)^{-1}$). Let us take the nucleus' radius to be 25 km; we cannot expect the ρ dependence of v to hold all the way to the surface, so we will estimate v at 5 kilometers above it, say $\rho = 30$ km. Assuming the dust is accelerated out to $\rho = 100$ km, v will be about $(100/30)^{0.7} = 2.3$ times smaller.

Now, the terminal velocity v_t of the dust grains at the time of the occultation was about 0.6 km/s. This is based on (a) v_t at perihelion ($r = 0.9$ AU) being about 1.0 km/s (Schleicher *et al.* 1998a), and (b) $v_t \propto r^{-0.41}$, which is a relation similar to that used for the speed of the gas in the coma (Biver *et al.* 1999). Therefore, at $\rho = 30$ km, $v \approx (0.6 \text{ km/s})/2.3 \approx 0.27$ km/s. Figure 12a of Gombosi *et al.* (1986) shows their model giving a 0.84-micron wide dust grain a speed of about 0.25 km/s at about 0.2 nuclear radii above the surface – equivalent in this case to $\rho \approx 30$ km. Since there are differences between Hale-Bopp's environment and that used in the model of Gombosi *et al.* (1986), and further their calculated v does not strictly follow $\rho^{0.7}$, this match between v is somewhat coincidental, but it is clear that v is roughly comparable to model calculations.

We noted the high optical depth implied by our modeling. Canonically, comae must be optically thin so that sunlight can reach the nucleus to drive the sublimation of gas, leading to the production of the dust in a self-regulating manner. However, an optically thick inner coma could be a secondary source for energy, via scattering of sunlight and thermal reradiation, especially if the dust has been superheated, as seems to be the case for Hale-Bopp (Lisse *et al.* 1999a). This problem has been analyzed by others, who have found by various analytic and numerical simulation methods that the energy deposited to the nucleus is a weak function of comatic

optical depth, even up to $\tau \sim 2$; reradiation almost compensates (or, in some analyses, over-compensates) for the decrease in sunlight (see, e.g., Salo [1988], Hellmich [1981]).

An important check is whether a high τ makes sense. We argue that it does, as follows. $Af\rho_o/\phi(\alpha)$, derived above, is 1.6 ± 0.2 km at $\rho_o = 100$ km. At the time of the *Giotto* flyby of comet 1P/Halley, Schleicher *et al.* (1998b) report that Halley's $Af\rho_o/\phi(\alpha) = 0.53$ km, and Keller *et al.* (1987) calculate from *Giotto* imaging that the peak opacity of the dust coma, a few kilometers above the surface of the nucleus, was about 0.3. So Hale-Bopp's $Af\rho_o/\phi(\alpha)$ from §IVc was at least 3 times larger than Halley's during the flyby. With the two comets' dust grains having roughly the same albedo, it is clear that it would be not be difficult for Hale-Bopp to have had a peak τ around unity. Furthermore, it is likely that Hale-Bopp's near nucleus $Af\rho_o/\phi(\alpha)$ was even higher, for the following reason. Our modeling shows the dust opacity profile to be proportional to $\rho_o^{-1.7\pm0.3}$ or so, making

$$Af\rho_o/\phi(\alpha) \propto \rho_o^{-0.7\pm0.3}. \tag{4.6}$$

This is not strictly true at the higher optical depths, since $f > 1$ is not allowed, but it does imply that $Af\rho_o/\phi(\alpha)$ is higher than the 1.6 km as one travels in from $\rho = 100$ km, so that it is probably more than three times larger than Halley's when measured near the nucleus' surface.

4.2.6 Summary of Occultation Results

We report constraints on the nuclear and comatic properties of Comet Hale-Bopp as implied by our observations of an occultation of a ninth-magnitude star. Except for the special case of Comet Chiron, this would be the first time such an event with so small an impact parameter has been observed. Our observations were marred by thin clouds and a lack of adequate corroborating data – only one chord through a sufficiently thick portion of the coma was apparently measured – but there are many pieces of circumstantial evidence to show that we indeed observed the occultation. Moreover, we know of no other observations of the comet that can refute our conclusions. Our data nearest the nucleus were collected about 800 km from the latest prediction, but this is not unreasonable since such a distance is comparable to the astrometric error in determining the nucleus' location within a finitelypixelized image dominated by comatic flux.

By modeling the shape of our light curve with a simple coma and spherical nucleus model, and assuming that our observation recorded the occultation, we find the following:

• 1. Assuming the power-law opacity profile of the coma, with exponent n, is as shallow as or shallower than 2.4, the impact parameter b is ≤ 45 km, but the best fits occur when $b \leq 33$ km. Our occultation observation has sampled the near-nuclear inner coma, which has only rarely been observed before in any comet.

• 2. If $n \leq 2$, the nucleus is spherical, and the coordinate origin is constrained as depicted in Fig. 4.5, then the nuclear radius R must be smaller than about 30 km. Relaxing the constraints on n yields an upper limit of 48 km.

• 3. The inner coma of Hale-Bopp is probably optically thick, even at nearly 3 AU from the Sun. Regardless of the values for the other parameters, good fits to the

data can only be found if the opacity within the first few tens of km of the center (not the surface) of the nucleus was at least unity. For some applicable models R is bigger than this distance, in which case the maximum coma opacity is less than one, but never much less.

• 4. We find that the albedo ($A/\phi(\alpha)$) of the dust, while it is within 100 km of the nucleus' center, is 0.21 ± 0.02 (formal error). The equivalent geometric albedo p is 0.05 ± 0.005 (formal error). This assumes that all photons within this region are doubly-scattered. Without this caveat, the calculated albedo is lower than the "typical" value ($p = 0.01$, compared to 0.03 from Divine *et al.* [1986]).

• 5. The dust opacity profile is probably steeper than the canonical ρ^{-1} power law, being most likely proportional to ρ^{-n} with $n \geq 1.4$. Marginal fits can be found for $n = 1.0$ for one hemisphere. (The other hemisphere is, in that case, quite steep, $n \approx 2$.) This occurs possibly within 160 or 170 km of the nuclear center, but definitely within 100 km. This chord through the coma may have sampled the acceleration region of the dust, and/or azimuthal variations in the inner coma, so our model, which describes the coma's density as two hemispheres each having a single power-law function of cometocentric distance, would be too simplistic.

• 6. The steepness of the profile in the deepest coma does not match that of the jet structure seen in large-scale images, although the resolution of all ground-based imaging fails to directly sample the 100-kilometer scales we are measuring via the occultation. The characteristic n for the wings of the occultation light curve could follow the same value as for the large-scale images and the processes mentioned in Item 5 above may only be important within the first 100 km of the coma.

4.3 Thermal Emission and Scattered Light Imaging

4.3.1 Observations

Table 4.5 lists the non-occultation data taken on comet Hale-Bopp, in the optical, mid-IR, and radio regimes. Heliocentric distance (r), geocentric distance (Δ), and phase angle (ϕ) are given, along with our measurement of the flux from the nucleus of the comet. In all observations except for the microwave, where the comet appeared as a point source, processing using the coma-fitting method from Chapter 3 was required to separate the comatic from the nuclear flux. One notices that unfortunately the image processing was inconclusive for many of the datasets. The brightness of the nucleus is stated using either its Cousins R magnitude or its flux in Janskys. (One Jansky is 10^{-26} W/m^2/sr/Hz.) Images from Apr 1997 (near perihelion) were too choked with coma to detect the nucleus; these data were used, however, to infer the nucleus' rotation period. The comet's coma during late November and December 1996, and July 1997 was not structured enough to allow an analysis with our method; these entries are italicized in the table.

4.3.2 Analysis

4.3.2.1 Infrared and Optical Data

We performed the coma-fitting analysis on our infrared and optical data sets, and we show some of the results in Figs. 4.8, 4.9, 4.10, 4.11 (optical), and 4.12

Table 4.5. Observations of Comet Hale-Bopp

No.	Date (UT)	System	Wavelength
1	23 Oct 1995	*HST* + WFPC2	6750 Å
2	20 May 1996	*HST* + WFPC2	6750 Å
3	22 Jun 1996	*HST* + WFPC2	6750 Å
4	17 Oct 1996	*HST* + WFPC2	6750 Å
5	31 Oct - 2 Nov 1996	ESO 3.6-m + TIMMI	11 μm
6	*30 Nov - 3 Dec 1996*	*ESO 3.6-m + TIMMI*	*11 μm*
7	*21 - 24 Jan 1997*	*NASA/IRTF + MIRAC*	*11 μm*
8	21 - 27 Mar 1997	VLA	3.55 cm
9	4 - 12 Apr 1997	NASA/IRTF + $\begin{smallmatrix}\text{MIRLIN}\\ \text{MIRAC}\end{smallmatrix}$	5-20 μm
10	*15 - 21 Jul 1997*	*ESO 3.6-m + TIMMI*	*11 μm*

Table 4.5 - Continued

No.	r (AU)	Δ (AU)	ϕ (deg)	Nuclear flux	CF?[a]	Rot?[b]
1	6.35	6.71	8.2	$R_C = 18.3 \pm 0.1$	Y	N
2	4.35	3.68	10.8	$R_C = 16.0 \pm 0.1$	Y	N
3	4.01	3.03	4.5	$R_C = 15.6 \pm 0.1$	Y	N
4	2.69	3.04	18.8	$R_C = 15.3 \pm 0.1$	Y	N
5	2.53-2.50	3.05	17.4-17.2	5.0 ± 0.5 Jy	Y	N
6	*2.16-2.12*	*2.93-2.91*	*13.9-13.7*	NA	N	N
7	*1.50-1.46*	*2.22-2.16*	*21.4-22.6*	NA	N	N
8	0.94-0.92	1.32	49.0-48.9	20 ± 3 μJy	NA[c]	N
9	0.92-0.93	1.38-1.47	46.6-42.5	NA	N	Y
10	*1.94-2.02*	*2.75-2.80*	*15.1-15.6*	NA	N	N

[a] "CF" = "Coma fitting." Are the data good enough to use the coma-fitting technique (Chapter 3)?

[b] "Rot" = "Rotation." Was the rotation period deriveable from the data?

[c] Image is a point-source – no coma seen.

(infrared). Each figure shows the analysis of one typical image from each of the five observing runs where the analysis was applicable. The upper left panel in each figure shows the original image, the upper right shows the model, the lower left shows the residual, and the lower right compares the residual's profile with that of a PSF. All images have used logarithmic scaling. The residual plot in each figure follows the profile of the PSF reasonably well.

For the four optical datasets, we find a consistent value for the nuclear cross section even though the inner coma of Hale-Bopp is thought to be optically thick, as explained in Section 4.2. It is possible that all three 1996 measurements show actually the cross section of the optically-thick portion of the coma rather than of the nucleus. Optical images from Oct 1995 offer the best chance to detect the nucleus without much intervening near-nuclear coma. The interpretation of the optical and mid-IR measurements of the nucleus will be explained below.

Infrared images taken near perihelion were useful in constraining the rotation period of the nucleus. Indeed, it was the only portion of the datasets that indicated this, since photometric determinations of the rotation were impossible. Morphological changes in the coma during the period of (UT) 4 Apr to 12 Apr 1997 were analyzed and it was found that the repeatability of the structure had a mean periodicity of $P = 11.30 \pm 0.05$ hr (1-σ) over that time period. The sequence of images is shown in Fig. 4.13. The rotational phase is written in each image of the sequence. I have a nine-hour sequence of images from 4 Apr and a five-hour sequence from 5 Apr, which have been combined to produce the 39-image sequence; this is the "MIR-LIN" sequence labelled on the figure. The two days limited the possible periods to P and $2P$. Subsequent imaging on 12 Apr – the "MIRAC" image on the figure – was matched with the first two days to remove the period ambiguity. The caveats to attaching a rotation period of the nucleus to the variability of coma morphology have been explained in Chapter 3.